Article

The Design of Piecewise Integrated Composite Bumper Beam With Machine Learning Algorithm

Seokwoo Ham and Seong S. Cheon *

Posted Date: 15 February 2023

doi: 10.20944/preprints202302.0257.v1

Keywords: Composite material; Bumper beam; Machine learning; Stacking sequence; Piecewise integrated composite

Article

The Design of Piecewise Integrated Composite Bumper Beam With Machine Learning Algorithm

Seokwoo Ham wand Seong S. Cheon *

Department of Mechanical Engineering, Kongju National University, Republic of Korea
* Correspondence: sscheon@kongju.ac.kr

Abstract: In the present study, piecewise integrated composite (PIC) bumper beam for passenger cars was proposed and design optimisation process for composite bumper beam against IIHS test was carried out with the help of machine learning. Several elements in IIHS bumper FE model have been assigned to be references, in order to collect training data which, allow the machine learning model to study the method of predicting loading types of each finite element. 2-D and 3-D implementations were provided by machine learning models, which determined stacking sequences of each finite element in PIC bumper beam. It was found that the PIC bumper beam, which was designed by machine learning model has direct impact on reducing the possibility of failure as well as increasing bending strength effectively than conventional composite bumper beam. Moreover, 3-D implementation produced better results compared with 2-D implementation since it was preferable to choose loading type information which was achieved from surroundings when the target elements were located either at corner or junction of planes instead of using information came from the same plane of target.

Keywords: Composite material; Bumper beam; Machine learning; Stacking sequence; Piecewise integrated composite

1. Introduction

Environmental issues have recently accelerated legislative actions worldwide targeting automotive industries and continuous demanding rigorous improvement for fuel efficiency, electric motor driving power system and structural compactness/lightness. Specifically, structural lightness is unceasingly required regardless of electric power system or capacity of auto-body, therefore, numerous works have been found so far. These works include topology optimisation, novel design methodologies and applying lightweight materials, such as non-ferrous light metals, thermoplastics, and fibre reinforced composites [1-4]. In particular, fibre reinforced composites have excellent specific strength, stiffness, and damping characteristics without sacrificing weight saving effect. Due to these beneficial properties, they have been used for structural materials of aircraft and space vehicles. As low-cost manufacturing technologies and mass production methods for composite structures have been established, the application of composite materials to leisure sport goods and auto-bodies are being increased nowadays [5-9].

Bumper beam is one of key parts in the vehicle to alleviate crash damages both for structure and passengers. Recent bumper beams are frequently made of composites in order to improve crashworthiness and structural lightness simultaneously. So far, entire region of composite bumper beams has been made based on conventional uni-style stacking sequences without changing sequences of composite plies or fibre orientations [10-13]. Jeong et al. [14] proposed a novel concept of PIC (Piecewise Integrated Composite), in which the loading type of bumper beam was analyzed and dissimilar stacking sequences, i.e., tension dominant, compression dominant and shear dominant, were assigned into five equally divided sub-regions of the composite bumper beam. However, intentionally divided sub-regions did not sufficiently reflect element-based dominant external loading types therefore, it is necessary to automatically assign dissimilar stacking sequences into each element to improve structural characteristics because each local part of the bumper beam is experiencing different types of loading during crash. Moreover, the best way to assign dissimilar stacking sequences into all elements is using machine learning technique. Accordingly, the PIC bumper beam design method with employing machine learning models was proposed in order to improve bending strength and structural lightweight effect of the product in the present study. Meanwhile, training data, which allow the machine learning model to study the method of predicting loading types of each finite element, were obtained from preliminary IIHS bumper beam FE analysis. Also, training data in the current study should contain information about stress triaxiality along with location in the form of coordinate values. Five different types of algorithms, which underlie on the machine learning model, were applied to guarantee the highest performance in view of improving bending strength and structural lightweight effect of the product [15-17]. Results of highest performance predicted loading type of each finite elements and robust stacking sequences against loading type were mapped into the entire region of bumper beam finite elements. Finally, the designed PIC bumper beam was verified in view of the strength improvement and structural weight saving effect by the IIHS bumper beam analysis.

2. Outline of the PIC Bumper Beam Design Process

The PIC is assigning different stacking sequences for each shell element with a size of 4mm×4mm as a similar form of mosaic and elements are assumed to have been perfectly bonded each other in order to increase robustness toward various external loading types. Firstly, a preliminary IIHS bumper FE analysis using aluminium bumper beam was carried out to achieve data, which are the input to machine learning model. For the material of the bumper beam during the preliminary FE analysis, aluminium alloy 7021 [18] was used since stress distribution within the beam is identical regardless of the material of the beam. Several elements among finite elements were chosen to be reference elements in order to collect stress triaxiality for judging the state of loading type, i.e., tension, compression, or shear with proper location. These data, resulted from reference elements, i.e., loading type and location were defined as training data, which are the input to machine learning model as explained previously.

Acquired training data are randomly assigned to five groups, i.e., each group contains 20% of training data for generalization’s sake [19]. One of groups is arbitrarily chosen for testing, the others for training which are put into machine learning algorithms, therefore, five times of trials are to be carried out per one iteration, which are known to be k-fold cross validation [20]. In the meantime, machine learning algorithms produce different performances according to their hyperparameter values. Mean value of accuracy and ROC (receiver operating characteristic)-AUC (area under the curve) are resulted from performance testing of machine learning algorithms. On condition that the results are not satisfactory, hyperparameters are tuned through the Bayesian optimisation algorithm and iterations are conducted until the lowest error or the highest performance is obtained. The iterative process, i.e., training group, machine learning algorithms, performance testing and hyperparameter tuning are known as machine learning model. When the results are acceptable, then loading types of unreferenced elements are able to be assigned and mapped into finite elements of the PIC bumper beam. Figure 1 shows the flowchart of PIC bumper beam design process.

doi:10.20944/preprints202302.0257.v1

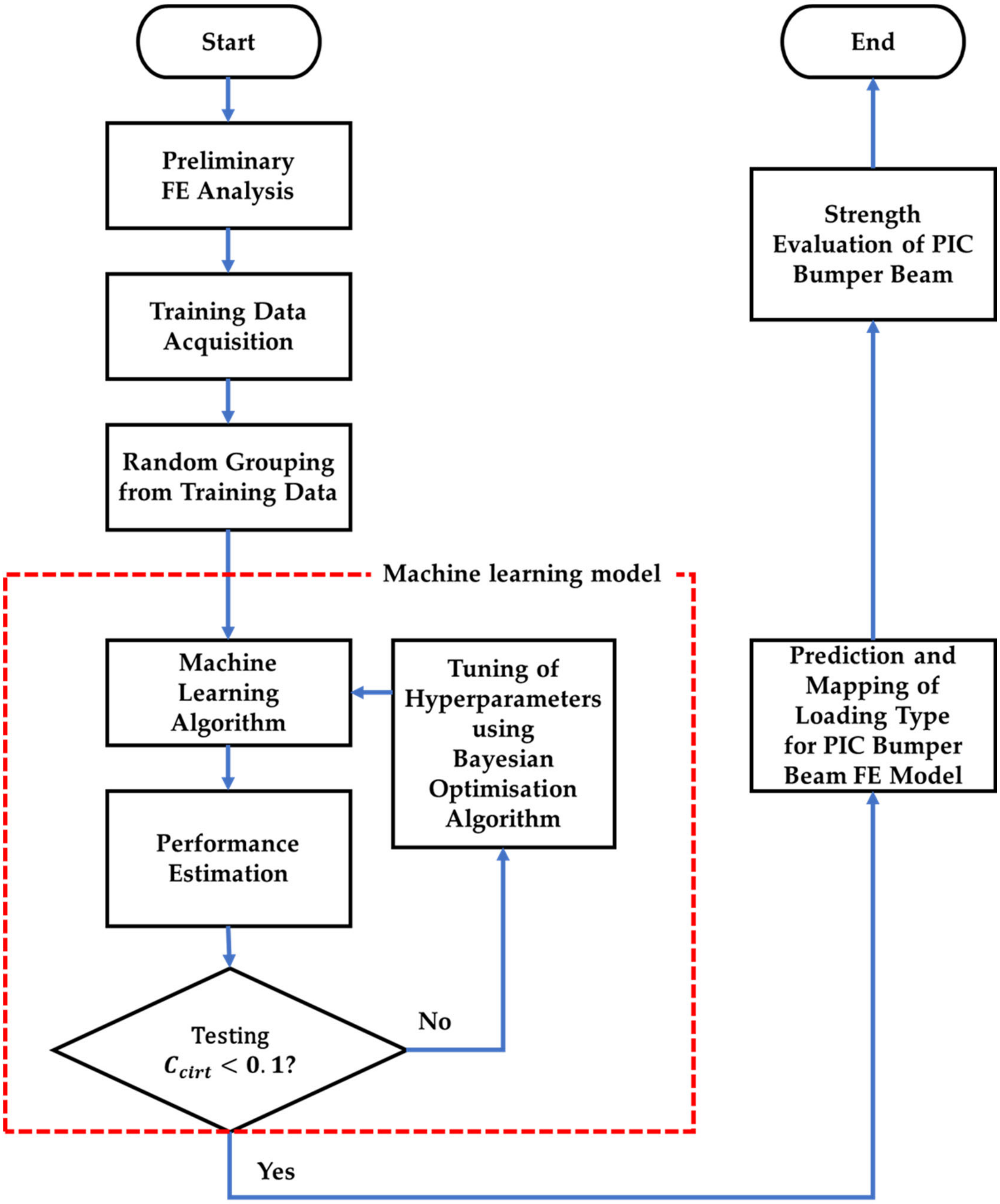
Start
Preliminary FE Analysis
Training Data Acquisition
Random Grouping from Training Data
Machine learning model
Machine Learning Algorithm
Tuning of Hyperparameters using Bayesian Optimisation Algorithm
Performance Estimation
Testing $C_{cirt} < 0.1?$
No
Yes
Prediction and Mapping of Loading Type for PIC Bumper Beam FE Model
Strength Evaluation of PIC Bumper Beam
End

Figure 1. Flowchart of PIC with machine learning model.

3. Preliminary IIHS Bumper FE Analysis

The FE analysis was conducted with ANSYS LS-DYNA (ANSYS, Inc.), one of representative explicit finite element programs. The Belytschko-Lin-Tsay shell formulation is known to be suitable for expressing nonlinear anisotropic behavior of thin shell structure including complex load and large deformation with saving computation time [21]. Also, it was possible to track the through the thickness directional stresses at the top, mid and bottom surfaces of each element when the number of integration points was set to be three. For that reason, Belytschko-Lin-Tsay four node shell element with three integration points through the thickness direction were selected in order to model the thin-walled structures of bumper beam. Material model, which is able to be used for an elasto-plastic characteristics with an arbitrary stress as a function of strain curve and arbitrary strain rate dependency, was selected [22].

As previously noted, aluminium alloy 7021 was used for the material of the bumper beam during the preliminary FE analysis. Mechanical properties of aluminium alloy 7021 were summarised in **Error! Reference source not found.**.

Table 1. Aluminium alloy 7021 mechanical properties.

Mechanical properties	Value
Density ρ	2,700 kg/m^3
Young's modulus	70 GPa
Poisson's ratio ν	0.3
Yield stress σ_y	360 MPa

About 13% of total finite element were assigned to be references, in order to collect stress triaxiality for judging the state of loading type with proper location during IIHS bumper simulation. Stress triaxiality and coordinate location values for each reference element was included in training data. Total number of elements in bumper beam is about 9,500 and the reference element ratio is 12.8%, which is 1,210. Figure 2 shows the finite element bumper beam model with indicating reference elements and the cross-section of the bumper beam. Cross-sectional shape, total length, and radius of curvature for the bumper beam were designed with regard to the current product which was installed in a passenger car of "A" company. 2,200kg of the vehicle weight was considered as a form of concentrated mass element in the IIHS bumper crash analysis [14]. The IIHS bumper test is representatively used to measure the damage regions during the low-speed crash. In the meantime, the deformable barrier was modelled with 39,800 number of elements, based on the IIHS bumper test protocol [23]. The FE model for an automotive bumper beam and an IIHS standard deformable barrier including bumper crash boxes was illustrated in Figure 3. Aluminium alloy 7021 was used for the material of the bumper crash box which was firmly connected to rectangular cross-sectional to both ends of the bumper beam. As indicated in Figure 3, the initial speed was 10 km/h, and the vehicle mass of 2,200 kg was given to the point, in which the real centre of gravity of a passenger car was located. Consequently, it was found that 505 number of reference elements in tension, 593 in compression, and 112 in shear among 1,210 reference elements.

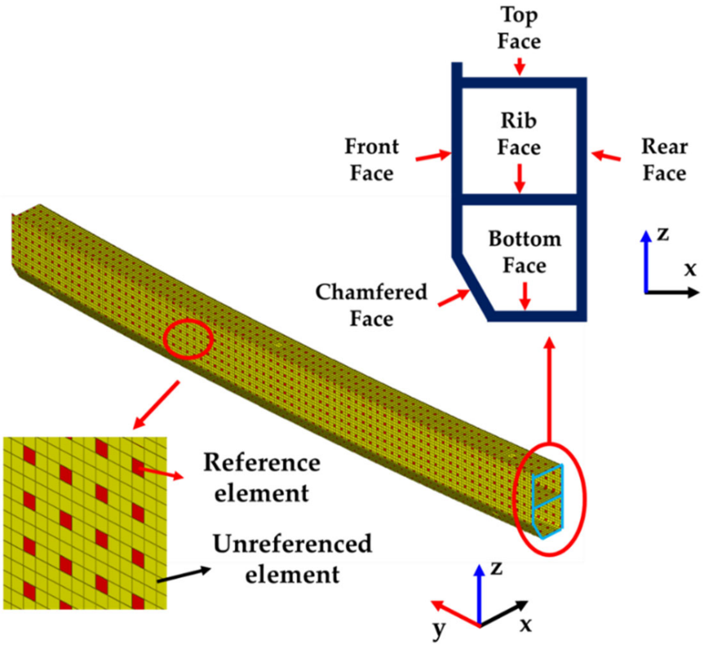

Figure 2. FE bumper beam model.

doi:10.20944/preprints202302.0257.v1

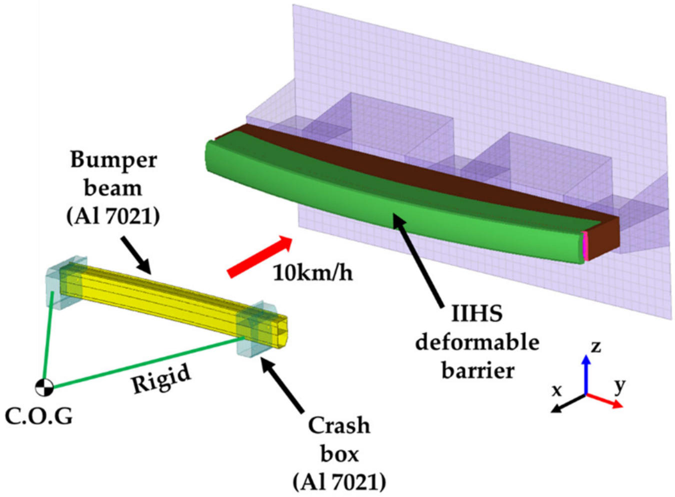

Figure 3. Preliminary IIHS bumper analysis boundary conditions.

4. Training Data Acquisition and Random Grouping

As previously mentioned, the training data, which consist of stress triaxialities and coordinate location values, were obtained from preliminary IIHS bumper beam FE analysis.

There are two different implementations methods for random grouping, i.e., 2-dimentional(2-D) implementation and 3-dimensional(3-D) implementation. When the 2-D implementation is used, the training data is obtained from each face of bumper, i.e., the training data for top, front, chamfered, bottom, rear, and rib faces, respectively. Each training data regulates its own face, i.e., training data, which is obtained from top face is used only for predicting loading type of reference elements located in top face, etc. Meanwhile, training data in any faces are able to be used for any faces, on 3-D implementation.

Loading type of reference elements is determined through the stress triaxiality of each element. The definition of the stress triaxiality, is shown in Eq. (1).

$$\eta = \frac{\sigma_m}{\bar{\sigma}} \tag{1}$$

where σ_m and $\bar{\sigma}$ are the mean principal stress and the von Mises stress, respectively [24]. Eqns. (2) and (3) show the definitions of mean principal stress and von Mises stress.

$$\sigma_m = \frac{(\sigma_x + \sigma_y + \sigma_z\ )}{3} \tag{2}$$

$$\bar{\sigma} = \sqrt{\frac{1}{2}\left[\left(\sigma_x - \sigma_y\right)^2 + \left(\sigma_y - \sigma_z\right)^2 + (\sigma_z - \sigma_x)^2 + 3\left(\sigma_{xy}^2 + \sigma_{yz}^2 + \sigma_{zx}^2\right)\right]} \tag{3}$$

When η is bigger than 0.1, loading type is considered to be tension dominant. Compression dominant loading type is believed if η is smaller than -0.1. In case η is bigger than -0.1 and smaller than 0.1, that element is subject to shear dominant loading [25].

Acquired training data are randomly divided into five groups, i.e., each group contains 20% of training data for the sake of generalization. As previously noticed, one of groups is arbitrarily chosen for testing, the others for training which are put into machine learning algorithms, therefore, five times of trials are to be carried out per one iteration, which are known to be k-fold cross validation.

5. Machine Learning Models

As previously mentioned in Ch.2, machine learning model consists of machine learning algorithms, performance estimation/testing and hyperparameter tuning.

5.1. Machine Learning Algorithms

Machine learning algorithms are able to characterise data for the sake of classification, regression, clustering, and outlier detection. In the present study, classification related machine learning algorithms were considered since it is indispensable to classify unknown data with decent prediction. Decision tree, ensemble decision tree (boosted and bagged), SVM (Support vector machine), and k-NN (k nearest neighbors) classification were chosen among classification algorithms according to their ability of classifying imbalanced data [26]. Each algorithm has several different parameters, i.e., hyperparameters, which are to be iteratively tuned based according to the Bayesian algorithm in order to optimise the results [27]. A detailed description of the classification used can be found as follows:

5.1.1. Decision Tree

Decision tree is normally used to compare unknown data to tree structure, which consists of root, branches and leaves. During the root process, unknown data are input to the decision tree algorithm and the output of the root process is transferred to various branches. Intermediate results for determining loading types of unknown data are generated based on the characteristics of training groups, which survive from criteria during the branch process. Final loading types of unknown data are unveiled in the leaf process. Decision tree has two hyperparameters, i.e., maximum number of splits and criteria, which was summarised in Table 2 [28].

Table 2. Decision tree hyperparameters.

Machine learning model	Hyperparameter	Variable
Decision tree	Max. number of splits	1~1209
	Split criterion	Gini's diversity index Towing rule Maximum deviance reduction

5.1.2. Ensemble Method

There is a high possibility that the overfitting, which is indicating that predicted results of loading types are sufficiently good for training group, however, poor prediction is generated for unreferenced elements, happens when it involves too much branch processes. To reduce the effect of overfitting, it is recommended to apply the ensemble method, which merges outcomes from several branches into one value. In the present study, boosted decision tree and bagged decision tree are considered since they are considered to be representative machine learning algorithms with ensemble method. The boosted decision tree is applying the same algorithm model, which is previously used for the decision tree, iteratively and sequentially. Iterations are conducted with updated weighting factor, until the results fulfil the criterion. It requires maximum number of splits, number of learners, and learning rate as its hyperparameters. Bagged decision tree needs to apply several decision trees, which are generated by bootstrapping variations of the same decision tree algorithm model, parallelly at the same time. The best result is selected among aggregated ones based on a majority vote. The bagged decision tree needs two hyperparameters, i.e., maximum number of splits and number of learners. Table 3 shows the hyperparameters for the ensemble method [29].

Table 3. Ensemble methods hyperparameters.

Machine learning model	Hyperparameter	Variable
Boosted decision trees	Max. number of splits	1 ~ 1209
	Number of learners	10~500
	Learning rate	0.001~1

Bagged decision trees	Max. number of splits	1 ~ 1209
	Number of learners	10 ~ 500

5.1.3. SVM

SVM aims at forming the finest suitable decision limit or boundary, known as hyperplane, which separates n-dimensional space into loading types, making it easy to place a different point in the appropriate area. In SVM algorithm, extreme vector points called support vectors are chosen which help in creating a proper hyperplane. Hyperplane of SVM is defined as the best possible decision boundary out of various possible decision boundaries that accurately classifies the classes in n-dimensional space. Features of the training group determine the dimensions of the hyperplane. A hyperplane having maximum margins, which means the distance between two data points is maximum, is preferred. Kernel function, kernel scale, box constraint level, and multiclass method are hyperparameters, which are listed in Table 4 [30].

Table 4. SVM hyperparameters.

Machine learning model	Hyperparameter	Variable
SVM	Kernel function	Gaussian Linear Quadratic Cubic
	Kernel scale	0.001~1000
	Box constraint level	0.001~1000
	Multiclass method	One-vs-One One-vs-All

5.1.4. k-NN Classification

The k-NN classification is instance-based learning method used to classify objects based on their closest training group in the feature space. An object is classified by a majority vote of its neighbors, i.e., the object is assigned to the class that is most common amongst its k-nearest neighbors, where k is a positive integer. In the k-NN classification, the classification of a new test feature vector is determined by the classes of its k-nearest neighbors. Here, the k-NN classification was implemented using various distance metrics to locate the nearest neighbor. Number of neighbors, distance metric, and distance weight are its hyperparameters as shown in Table 5 [31].

Table 5. k-NN classification hyperparameters.

Machine learning model	Hyperparameter	Variable
k-NN classification	Number of neighbors	1 ~ 605
	Distance metric	City block Chebyshev Correlation Cosine Euclidean Hamming
	Distance weight	Equal Inverse Squared inverse

5.2. Performance Testing

There are four types of cross validations, i.e., k-fold, holdout, leave-p-out and leave-one-out in order to estimate the performance of the machine learning algorithms [32]. In the present study, k-fold cross validation was selected among them since it is known to have an ability to reduce biases and classify loading types with low capacity of training data [33]. As mentioned in Ch. 2, acquired training data were randomly divided into five groups, i.e., each group contains 20% of training data for the sake of generalization. One of groups was arbitrarily chosen for testing, the others for training which were put into machine learning algorithms, therefore, five times of trials were carried out per one iteration.

The performance of the machine learning algorithms was estimated using the accuracy and the ROC-AUC value [34]. Accuracy is the proportion of correct predictions made by the model out of the total number of predictions as shown in Eqn. (4) [35].

$$Accuracy\ (\%) = \frac{Number\ of\ correct\ predictions}{Total\ number\ of\ predictions} \times 100 \tag{4}$$

Accuracy is a widely used metric because of its simplicity and effectiveness, however, it contains the mixed information of tension, compression, and shear loading types. According to the possibility of imbalanced training data, which were produced from preliminary FE analysis, ROC-AUC might alleviate the misleading results by the imbalanced data [36]. ROC-AUC is suitable for estimating imbalanced loading type data, since they can separately show individual values for each loading type among training group. The ROC curve comes from ratios based on correctly predicted data and incorrectly predicted data, and the AUC means the area under the ROC curve. Generally, AUC takes values from 0 to 1, where a value of 0 indicates a perfectly inaccurate estimation, and a value of 1 reflects a perfectly accurate estimation. Less than 0.5 of AUC value suggests no discrimination, 0.7 to 0.8 is considered acceptable, 0.8 to 0.9 is considered excellent, and more than 0.9 is considered outstanding [37, 38]. The convergence criterion (C_{crit}) is defined as the change in accuracy as shown in Eqn. (5) [39].

$$C_{crit} = \left|\frac{A_n - A_{n-1}}{A_n}\right| \tag{5}$$

where A_n implies the accuracy value at the n- iteration. In order to meet the highest performance, the value for the convergence criterion was set to be 0.1. When the results were not satisfactory, hyperparameters were tuned based on Bayesian optimisation algorithm and iterative performance estimation and testing were conducted, which was detailed in the next chapter.

5.3. Hyperparameter Tuning with Bayesian Optimisation Algorithm

As previously mentioned, hyperparameters are tuned through the Bayesian optimisation algorithm, which is famous for more effective compared to the grid search or random search, and iterations are conducted until the lowest error or the highest performance is obtained on condition that the results are not satisfactory [40, 41]. The main feature of optimising technique is to maximise the objective function, which is denoted by $\boldsymbol{f}$ along with hyperparameters as its independent variables. The output of the objective function is the performance of machine learning algorithms. Each iteration needs updating or tuning the hyperparameters within their own domain, which is represented by $\boldsymbol{X}$. Accordingly, the Bayesian optimisation algorithm can be explained as Eqn. (6):

$$\boldsymbol{x}^{*} = \arg\max_{\boldsymbol{x}\in\boldsymbol{X}} \boldsymbol{f}(\boldsymbol{x}) \tag{6}$$

where $\boldsymbol{x}$ denotes a set of hyperparameter values in the domain $\boldsymbol{X}$, and $\boldsymbol{x}^{*}$ is the set of hyperparameters that maximises the performance, i.e., the output of the objective function $\boldsymbol{f}$ [42]. Hyperparameters were tuned by the Expected-Improvement-Per-Second Plus, which provided fastest speed of the convergence criterion as well as prevented overexploiting possible ranges of hyperparameter domains from being illuded by the local maximum [43]. When the value of the convergence criterion became lower than 0.001, hyperparameter tuning was completed. Table 6 indicates the completely tuned hyperparameter values, which maximised the performance of each algorithm. Learning rate in the Boosted decision trees, Kernel scale and box constraint level of SVM were displayed by four decimal point.

Table 6. Optimised hyperparameter using Bayesian algorithms.

Machine learning model	Hyperparameter	Values
Decision tree	Max. number of splits	17
	Split criterion	Gini's diversity index
Boosted decision trees	Max. number of splits	1149
	Number of learners	50
	Learning rate	0.8987
Bagged decision trees	Max. number of splits	694
	Number of learners	214
SVM	Kernel function	Gaussian
	Kernel scale	30.2498
	Box constraint level	3.8962
	Multiclass method	One-vs-One
k-NN classification	Number of neighbors	4
	Distance metric	City block
	Distance weight	Squared inverse

Tables 7 & 8 show the highest performances, i.e., accuracy and ROC-AUC value of 2-D and 3-D implementations. All values in the Table 7 are the average of values of top, front, chamfered, bottom, rear, and rib faces both for the accuracy and the ROC-AUC. The accuracy from the 3-dimensional implementation was higher than that of the 2-dimensional implementation. The k-NN classification showed the highest accuracy both for 2-dimensional and 3-dimensional implementations. As shown in Tables 7 & 8, predicted ROC-AUC values for shear dominant loading type were smallest compared with either tensile or compressive ones, since the portion of shear dominant reference elements was lowest.

Table 7. Performances of 2-dimensional implementation.

Machine learning model	Accuracy (%)	ROC-AUC		
		Tension	Compression	Shear
Tree	84.2	0.85	0.88	0.73
Boosted decision trees	85.1	0.89	0.92	0.75
Bagged decision trees	81.1	0.90	0.91	0.75
SVM	85.9	0.89	0.90	0.62
k-NN classification	86.0	0.90	0.92	0.75

Table 8. Performances of 3-dimensional implementation.

Machine learning model	Accuracy (%)	ROC-AUC		
		Tension	Compression	Shear
Tree	85.4	0.95	0.94	0.80
Boosted decision trees	85.1	0.98	0.97	0.87
Bagged decision trees	85.3	0.98	0.97	0.87
SVM	86.2	0.96	0.94	0.62
k-NN classification	86.3	0.98	0.97	0.87

6. Prediction and Mapping of Loading Type of Unreferenced Elements

k-NN was applied to predict loading types of unreferenced finite elements in the PIC bumper beam with the input of coordinate location values of target locations since it was revealed to be the most excellent classification both for 2-D and 3-D implementations from the comparison of resultant performance of machine learning algorithms without further predictions using other machine learning algorithms. In the meantime, there are no previous results of loading types for unreferenced elements, i.e., no solutions are existing, it was unnecessary to calculate either accuracy or ROC-AUC values. Predicted results involved loading types and their locations, for unreferenced elements, therefore, they were mapped into the PIC bumper FE model. In the meantime, robust stacking sequences against each loading type were listed in Table 9 [44]. Also, these stacking sequences were mapped into the FE model as shown in Figure 4.

Table 9. Robust stacking sequences against each loading type.

Dominant loading	Stacking sequence
Tension	$[\,90/\,0/\,\bar{0}]_{6s}$
Compression	$[\,\pm 5\,/\,\pm 45\,/\,90\,]_{3s}$
Shear	$[\,0/90]_{15}$

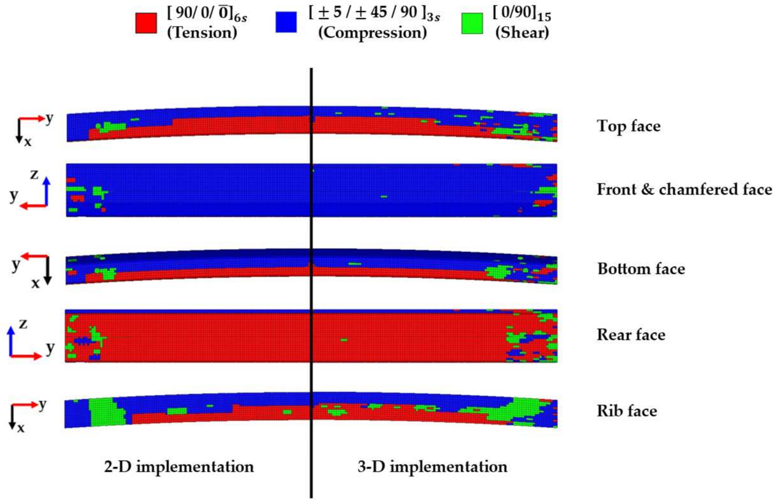

Figure 4. Mapping results - 2-D implementation vs 3-D implementation.

While machine learning algorithms were predicting dominant loading type at a certain face, only training data obtained from reference elements which were located at the same face during 2-D implementation. On the other hand, training data from reference elements, which were located at various faces depending on the metric values, were used for dominant loading type prediction in 3-D implementation as previously mentioned. From the Figure 4, it was observed that three different loading types were mixed together at both ends which were firmly connected to rectangular cross-sectional bumper crash boxes. 42.3%, 53.2%, and 4.5% of tension, compression, and shear dominant loading types were predicted for the entire PIC bumper beam FE model from 2-D implementation, whilst 42.1%, 50.4%, and 7.5% of tension, compression, and shear dominant loading types from 3-D implementation for the same bumper beam FE model. Also, each loading type areal difference was conspicuous in the rib face, i.e., tension dominant area from 3-D was 6.5% larger than that from 2-D, compression dominant area from 3-D was 12.5% smaller than that from 2-D, and shear dominant area from 3-D was 5.9% larger than that from 2-D, as observed from Figure 4. Meanwhile, loading type areas were the most similar from 2-D and 3-D on the front face. These results were summarised in Table 10.

Table 10. Predicted dominant loading type – 2-D implementation vs 3-D implementation.

Face	2-D implementation			3-D implementation		
	Tension	Comp.	Shear	Tension	Comp.	Shear
Top	43.5%	53.3%	3.2%	41.2%	50.2%	8.6%
Front & chamfered	0.8%	97.5%	1.8%	2.1%	95.9%	2.0%
Bottom	20.7%	30.4%	2.1%	15.8%	29.5%	7.9%
Rear	95.5%	2.0%	2.5%	92.0%	2.8%	5.2%
Rib	30.0%	54.4%	15.6%	36.6%	41.9%	21.5%
Total	42.3%	53.2%	4.5%	42.1%	50.4%	7.5%

7. Bending Strength Evaluation of PIC Bumper Beam

IIHS bumper analyses were performed using ANSYS LS-DYNA (ANSYS, inc.) in order to evaluate the bending strength of the PIC bumper beam based on the 2-D and 3-D implementations with employing machine learning model as well as a composite bumper beam with a conventional stacking sequence of $[0/\pm45]_{5S}$ for comparison's sake. Fully integrated shell formulation was selected to express nonlinear anisotropic behaviour with warpage under the function of improved transverse shear treatment for composite beam FE model [45]. Enhanced composite damage type material model, which are frequently used for describing material anisotropy with the help of the laminated shell theory, was selected for the whole composite part [22]. Table 11 shows the mechanical properties of T700/2510 carbon fibre epoxy composite which were considered for the composite bumper beam [46]. Initial velocity, vehicle weight and miscellaneous details were the same as those used in preliminary IIHS bumper beam FE analysis. Deformation of PIC bumper beam and crash box was illustrated in Figure 5.

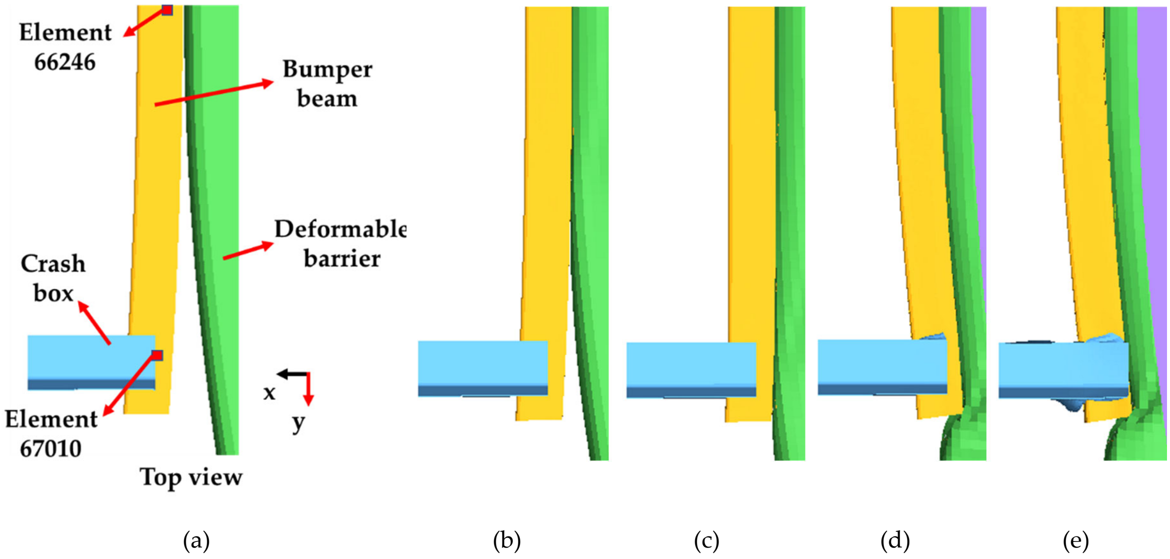

Figure 5. Deformation of PIC bumper beam (3-D implementation): (a) Time: 0 s, COG displacement: 0 mm, (b) time: 0.009 s, COG displacement: 24 mm, (c) time: 0.02 s, COG displacement: 54mm (d): time: 0.035 s COG displacement: 80 mm, (e) time: 0.045 s, COG displacement: 107 mm.

Beam was undergoing two types of deformation, i.e., bending type at centre part and buckling type along with cross-sectional direction at both ends which were connected to crash box. From Figure 5 (b), pure bending deformation of bumper beam was observed until 0.009 sec (C.O.G displacement: 24 mm), while buckling type crash box deformation started at 0.02 sec (C.O.G displacement: 54 mm) as shown in Figure 5 (c). Deformation of crash box initiated from the inner part and propagated to outer part owing to convex shape of the IIHS barrier. Bumper beam deformed to become a straight shape with respect to longitudinal direction and main deformation belonged to crash box at 0.035 sec (C.O.G displacement: 80 mm) as depicted in Figure 5 (d). In Figure 5 (e), maximum deformation of the bumper beam and crash box occurred at 0.045 sec (C.O.G displacement: 107 mm), elastic spring back started from this point.

Tsai-Wu indexes were investigated for specific elements, which were exposed to comparatively higher loading. The 66246th element and the 67010th element were chosen from the centre part and the RH end part of the composite bumper beam as visible in Figure 5 (a) since these parts underwent severer deformation during FE analyses.

Dominant loading type for the 66246th element and the 67010th element were found to be shear, and decent loading type was predicted by the 3-D implementation, but the 2-D implementation predicted compression for the elements. As a result, the Tsai-Wu indexes for the 66246th element and the 67010th element were shown in Figure 6.

Table 11. Mechanical properties of T700/2510 carbon epoxy composite [46].

Properties	Values
Density, $[\rho]$	1520 kg/m^3
Longitudinal modulus, $[E_1]$	126 GPa
Transverse Modulus, $[E_2]$	8.4 GPa
Shear modulus, $[G_{12}]$	4.23 GPa
Shear modulus, $[G_{23}]$	4.23 GPa
Poisson's ratio, $[v_{12}]$	0.024
Axial tensile strength, $[X^t]$	2172 MPa
Axial compressive strength, $[X^c]$	1450 MPa
Transverse tensile strength, $[Y^t]$	49 MPa
Transverse compressive strength, $[Y^c]$	199 MPa
In-plane shear strength, $[S]$	155 MPa

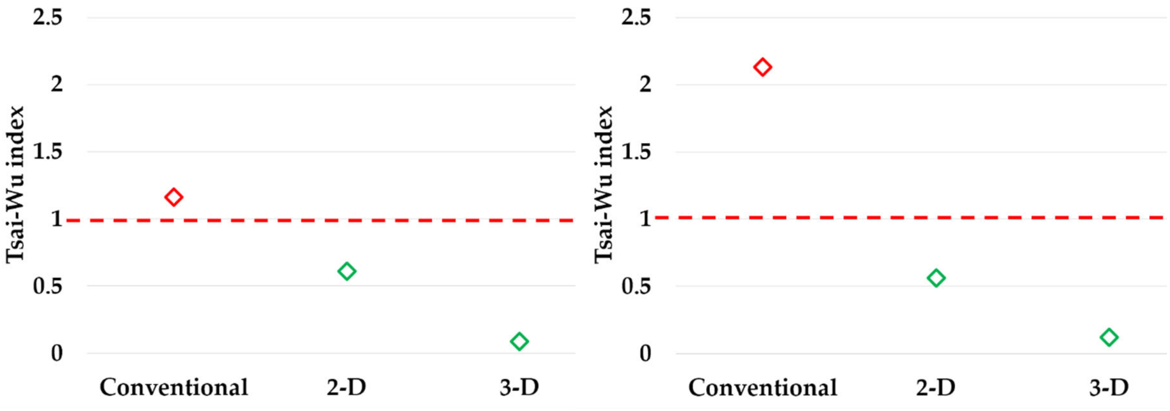

(a)

(b)

Figure 6. Tsai-Wu index: (a) Centre part (element 66246), (b) end part (element 67010).

In Figure 6, the index, calculated based on the conventional composite beam, was found to be exceeding 1. The index for 2-D was close to 1, but the index for 3-D was the lowest, i.e., conventional composite beam was experiencing fracture, while PIC bumper beams were safe under the same level of external loading. It was found that the conventional stacking sequence did not sufficiently respond to external loading, and the PIC bumper beams were safe and effective. In the meantime, the Tsai-Wu indexes revealed that the PIC beam of 3-D implementation was safer compared with that of 2-D implementation. The force-displacement curve results of conventional composite bumper beam and PIC bumper beams were plotted in Figure 7. Each deformation of stage (a), (b), (c), (d), and (e) in Figure 5 were synchronised to points from (a) to (e) in Figure 7.

Force slope increased at point (d) because crash boxes and both end parts of composite bumper beam started to deform. Higher external load resisting ability of a composite bumper beam was dependent on the proper stacking sequences of both end parts.

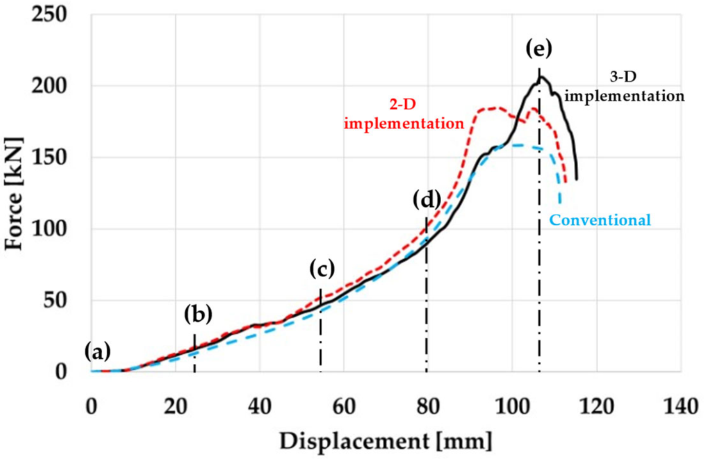

Figure 7. Force-displacement curve of composite bumper beams.

The maximum bending strength of the conventional composite bumper beam was 158 kN, while that of the PIC bumper beam based on 2-D implementation was 184 kN, and 3-D implementation, 206 kN, i.e., the bending strength of PIC bumper beam of 3-D implementation was about 10.4% and 23.0% higher than that of 2-D implementation and that of conventional stacking sequence, respectively. The PIC bumper beams with machine learning model showed superior bending strength to conventional composite bumper. As previously observed, PIC bumper beam of 3-D implementation showed higher external load resisting ability compared to that of 2-D implementation. Therefore, it was found that the 3-D implementation was more effective to assign proper stacking sequences into exact places of composite bumper beam. If PIC bumper beams were designed targeting the same bending strength level of conventional composite bumper beam, 8% and 12% of weight saving effects could be achieved as summarised in Table 12.

Table 12. Mass of same bending strength level composite bumper beam.

Design method	Bumper beam mass(kg)	(%)
Conventional	1.31	-
2-D implementation	1.20	8%↓
3-D implementation	1.15	12%↓

From crashworthiness point of view, conventional composite bumper beam absorbed 6980 J during IIHS bumper crash analysis. Meanwhile, 2-D implemented, and 3-D implemented PIC bumper beams absorbed 8230 J and 8260 J, respectively. PIC bumper beam of 3-D implementation also showed slightly higher energy absorption characteristics than either conventional or 2-D implemented composite bumper beam. Therefore, PIC bumper beam design with machine learning has direct impact on reducing the possibility of failure as well as increasing bending strength effectively. Moreover, 3-D implementation produced better results compared with 2-D implementation since it was preferable to choose loading type information which was achieved from surroundings when the target elements were located either at corner or junction of planes instead of using information came from the same plane of target.

8. Conclusions

The PIC bumper beam with employing machine learning models was proposed in order to improve bending strength and structural lightweight effect, which were proved by IIHS bumper FE simulations. During simulation, composite bumper beam was undergoing two major types of deformation, i.e., bending type at centre part and buckling type along with cross-sectional direction at both ends which were connected to crash box. 2-D and 3-D implementations were provided by machine learning models, which determined stacking sequences of each finite element in PIC bumper beam. It was found that PIC bumper beams were safe and effective, however, the conventional composite bumper beam did not sufficiently withstand external loading. In the meantime, the Tsai-Wu indexes revealed that the PIC beam of 3-D implementation was safer compared with that of 2-D implementation. Also, dominant loading type for centre part and both end parts were found to be shear, and correct loading type was predicted by 3-D implementation, but the 2-D implementation predicted compression for parts.

Bending strength of 3-D implementation was about 10.4% and 23.0% higher than that of 2-D implementation and that of conventional stacking sequence. PIC bumper beam of 3-D implementation showed higher external load resisting ability compared to that of 2-D implementation. Therefore, it was found that the 3-D implementation was more effective to assign proper stacking sequences into exact places of composite bumper beam. If PIC bumper beams were designed targeting the same bending strength level of conventional composite bumper beam, 8% and 12% of weight saving effects could be achieved. Therefore, PIC bumper beam design with machine learning has direct impact on reducing the possibility of failure as well as increasing bending strength effectively.

From crashworthiness point of view, conventional composite bumper beam absorbed 6980 J during IIHS bumper crash analysis. Meanwhile, 2-D implemented, and 3-D implemented PIC bumper beams absorbed 8230 J and 8260 J, respectively. PIC bumper beam of 3-D implementation also showed slightly higher energy absorption characteristics than either conventional or 2-D implemented composite bumper beam. Moreover, 3-D implementation produced better results compared with 2-D implementation since it was preferrable to choose loading type information which was achieved from surroundings when the target elements were located either at conner or junction of planes instead of using information came from the same plane of target.

Author Contributions: Conceptualization, S.W.H and S.S.C.; methodology, S.W.H and S.S.C.; software, S.W.H and S.S.C.; validation, S.W.H and S.S.C.; formal analysis, S.W.H and S.S.C.; data curation, S.W.H.; writing—original draft preparation, S.W.H and S.S.C.; writing—review and editing, S.W.H and S.S.C.; visualization, S.W.H and S.S.C.; investigation, S.W.H and S.S.C.; resources, S.W.H and S.S.C.; project administration, S.S.C.; funding acquisition, S.S.C. All authors have read and agreed to the published version of the manuscript.

Funding: This research was supported by Basic Science Research Program through the National Research Foundation of Korea (NRF) funded by the Ministry of Education (NRF-2018R1D1A1B07051169). Also, this work was supported by the research grant of the Kongju National University in 2020.

Institutional Review Board Statement: Not applicable.

Informed Consent Statement: Not applicable.

Data Availability Statement: Not applicable.

Conflicts of Interest: The authors declare no conflict of interest.

References

1. Bruggia, M.; Milanib, G. Optimal FRP reinforcement of masonry walls out-of-plane loaded: A combined homogenization–topology optimization approach complying with masonry strength domain. *Comput Struct* **2015**, 153, 49-74. https://doi.org/10.1016/j.compstruc.2015.02.004

doi:10.20944/preprints202302.0257.v1

2. Mirzendehdel, A.M.; Suresh, K., Support structure constrained topology optimization for additive manufacturing. *Comput Aided Des* **2016**, 81, 1-13. https://doi.org/10.1016/j.cad.2016.08.006
3. Gholizadeh, S.; Ebadijalal, M. Performance based discrete topology optimization of steel braced frames by a new metaheuristic. *Adv Eng Softw* **2018,** 123, 77-92. https://doi.org/10.1016/j.advengsoft.2018.06.002
4. Eckrich, M.; Arrabiyeh, PA; Dlugaj, AM; May, D. Structural topology optimization and path planning for composites manufactured by fiber placement technologies. *Comput Struct* **2022**, 289, 115488. https://doi.org/10.1016/j.compstruct.2022.115488
5. Slater, C.; Otto, SR; Strangwood, M. The quasi-static and dynamic testing of damping in golf clubs shafts fabricated from carbon fibre composites. *Procedia Eng* **2010**, 2, 3361-3366. https://doi.org/10.1016/j.proeng.2010.04.158
6. Kong, CD.; Lee, HS; Park, HB. Design and manufacturing of automobile hood using natural composite structure. *Compos B Eng* **2016**, 91,18-26. https://doi.org/10.1016/j.compositesb.2015.12.033
7. Colonna, M.; Bon, FD.; Tarterini, F.; Moncalero, M.; Totaro, G.; Gioia, C.; Fabbri, P. Ski Boot Soles Based on a Glass Fiber/Rubber Composite with Improved Grip on Icy Surfaces. *Procedia Eng* **2016**, 147, 372-377. https://doi.org/10.1016/j.proeng.2016.06.316
8. Muflikhun, MA.; Yokozeki, T. Experimental and numerical analysis of CFRP-SPCC hybrid laminates for automotive and structural applications with cost analysis assessment. *Compos Struct* **2021**, 263, 113707. https://doi.org/10.1016/j.compstruct.2021.113707
9. Kulhan, T.; Kamboj, A.; Gupta, N.K.; Somani, N. Fabrication methods of glass fibre composites-a review. *Funct. Compos. Struct* **2022**, 4, 022001. https://doi.org/10.1088/2631-6331/ac6411
10. Cheon, S.S.; Choi, J.H.; Lee, D.G.; Development of the Composite Bumper Beam for Passenger Cars. *Compos Struct* **1995**, 32, 491-499. https://doi.org/10.1016/0263-8223(95)00078-X
11. Hosseinzadeh, R.; Shokrieh, M.M.; Lessard, L.B. Parametric Study of Automotive Composite Bumper Beams Subjected to Low-velocity Impacts. *Compos Struct* **2005**, 68, 419-427. https://doi.org/10.1016/j.compstruct.2004.04.008
12. Belingardi, G.; Beyene, A.T.; Koricho, E.G. Geometrical Optimization of Bumper Beam Profile Made of Pultruded Composite by Numerical Simulation. *Compos Struct* **2013**, 102, 217-225. https://doi.org/10.1016/j.compstruct.2013.02.013
13. Kim, D.H.; Kim, H.G.; Kim, H.S. Design Optimization and Manufacture of Hybrid Glass/carbon Fiber Reinforced Composite Bumper Beam for Automobile Vehicle. *Compos Struct* **2015**, 131, 742-752. https://doi.org/10.1016/j.compstruct.2015.06.028
14. Jeong, C.H.; Oh, H.S.; Ham, S.W.; Kim, G.S.; Son, S.N.; Cho, Y.S.; Cheon, S.S. Crash simulation of a piecewisely-integrated composite bumper beams. *Int. j. mech. prod. eng.* **2018**, 6, 37-40.
15. Liang, L.; Sun, B. A Proof of Concept Study of Using Machine-Learning in Artificial Aortic Valve Design: From Leaflet Design to Stress Analysis. *Bioengineering (Basel)* **2019**, 6, 104. https://doi.org/10.3390/bioengineering6040104
16. Zhenchao, Q.; Nanxi, Z.; Yong, L.; Wenliang, C. Prediction of mechanical properties of carbon fiber based on cross-scale FEM and machine learning. *Compos Struct* **2019**, 212, 199-206. https://doi.org/10.1016/j.compstruct.2019.01.042
17. Hürkamp, A.; Gellrich, S.; Ossowski, T.; Beuscher, J.; Thiede, S.; Herrmann, C.; Dröder, K. Combining Simulation and Machine Learning as Digital Twin for the Manufacturing of Overmolded Thermoplastic Composites. *J. Manuf. Mater. Process.* **2020**, 4, 92.
18. Tisza, M.; Czinege, I, Comparative study of the application of steels and aluminium in lightweight production of automotive part. *Int. j. lightweight mater. manuf.* **2018**, 1, 229-238. https://doi.org/10.1016/j.ijlmm.2018.09.001
19. Arbameri, A.; Blaschke, T.; Chowdhuri, I.; Saha, A.; Chakrabortty, R.; Lee, S; Band, S. S, Ensemble of Machine-Learning Methods for Predicting Gully Erosion Susceptibility. *Remote Sens.* **2020**, 12(22), 3675. https://doi.org/10.3390/rs12223675
20. Saha, A.; Pal, S.C.; Chowdhuri, I.; Islam, A.R.M.T.; Roy, P.; Chakrabortty, R, Land degradation risk dynamics assessment in red and lateritic zones of eastern plateau, India: A combine approach of K-fold CV, data mining and field validation. *Ecol. Inform.* **2022**, 69, 101653. https://doi.org/10.1016/j.ecoinf.2022.101653
21. Key, S.W.; Hoff, C.C., An improved constant membrane and bending stress shell element for explicit transient dynamics, *Comput. Methods. Appl. Mech. Eng.* **1995**, 124, 33-47. https://doi.org/10.1016/0045-7825(95)00785-Y
22. LS-DYNA manual R13.0 Vol II. Available online: https://www.dynasupport.com/manuals/ls-dyna-manuals/ls-dyna_manual_volume_ii_r13.pdf (accessed on 9th Jan. 2023)
23. Bumper test and rating protocol (Version VIII). Insurance institute for highway safety: https://www.iihs.org/media/07bf4085-8c25-4972-aa56-c06ff19dae05/L5AzKw/Ratings/Protocols/archive/test_protocol_bumper_vVIII_0910.pdf (28. Nov. 2022)

24. Bai, Y.; Wierzbicki, T., Application of extended Mohr-Coulomb criterion to ductile fracture. *Int. j. Fract.* **2010**, 161, 1-20. https://doi.org/10.1007/s10704-009-9422-8
25. Bai, Y.; Wierzbicki, T. A new model of metal plasticity and fracture with pressure and Lode dependence. *Int. j. Plast.* **2008**, 24, 1071-1096. https://doi.org/10.3390/jmmp4030092
26. Bansal, M.; Goyal, A.; Choudhary, A, A comparative analysis of K-Nearest Neighbor, Genetic, Support Vector Machine, Decision Tree, and Long Short Term Memory algorithms in machine learning. *Decis. Anal.* **2022**, 3, 100071. https://doi.org/10.1016/j.dajour.2022.100071
27. Fakhrmoosavi, F.; Kamjoo, E.; Kavianipour, M.; Zockaie, A.; Talebpour, A.; Mittal, A., A Stochastic Framework Using Bayesian Optimization Algorithm to Assess the Network-level Societal Impacts of Connected and Autonomous Vehicles. *Transp. Res. Part C Emerg. Technol.* **2022**, 136, 103663. https://doi.org/10.1016/j.trc.2022.103663
28. Roy, S.; Mondal, S.; Ekbal, A.; Desarkar, M.S. Dispersion Ratio based Decision Tree Model for Classification. *Expert Syst. Appl.* **2019**, 116, 1-9. https://doi.org/10.1016/j.eswa.2018.08.039
29. Petković, M.; Ceci, M.; Pio,G.; Škrlj, B; Kersting, K.; Džeroski, S., Relational tree ensembles and feature rankings. *Knowl. Based Syst.* **2022**, 5, 109254. https://doi.org/10.1016/j.knosys.2022.109254
30. Richhariya, B.; Tanveer, M. EEG signal classification using universum support vector machine. *Expert Syst. Appl.* **2018**, 106, 169–182. https://doi.org/10.1016/j.eswa.2018.03.053
31. Xiao, J. SVM and KNN ensemble learning for traffic incident detection. *Physica A* **2019**, 517, 29–35.
32. Valente, G.; Castellanos, A.L.; Hausfeld, L.; Martino, F.; Formisano, E., Cross-validation and permutations in MVPA: Validity of permutation strategies and power of cross-validation schemes. *Neuroimage* **2021**, 238, 118145. https://doi.org/10.1016/j.neuroimage.2021.118145
33. Anandan, B.; Manikandan, M., Machine learning approach with various regression models for predicting the ultimate tensile strength of the friction stir welded AA 2050-T8 joints by the K-Fold cross-validation method. *Mater. Today Commun.* **2023**, 34, 105286. https://doi.org/10.1016/j.mtcomm.2022.105286
34. Raschka, S.; Mirjalili, V. *Python Machine Learning*, 2nd ed.; Packt Publishing: Birmingham, UK, 2019; pp. 230-240.
35. Papalampidou, A.; Papoutsi, E.; Katsaounou, P.A., Pulmonary nodule malignancy probability: a diagnostic accuracy meta-analysis of the Mayo model. *Clin. Radiol.* **2022**, 77, 443-450. https://doi.org/10.1016/j.crad.2022.01.055
36. Gajowniczek, K.; Ząbkowski, T. ImbTreeAUC: An R package for building classification trees using the area under the ROC curve (AUC) on imbalanced datasets. *SoftwareX* **2021**, 15, 100755. https://doi.org/10.1016/j.physa.2018.10.060
37. Mandrekar, J.N., Receiver Operating Characteristic Curve in Diagnostic Test Assessment. *J. Thorac. Oncol.* **2010**, 5(9), 1315-1316. https://doi.org/10.1097/JTO.0b013e3181ec173d
38. Hosmer, DW.; Lemeshow, S. *Applied Logistic Regression*, 2nd ed.; John Wiley and Sons: New York, USA, 2000; pp. 160-164.
39. Querin, O.; Victoria, M; Alonso, C.; Loyola, R.; Montrull, P. *Topology Design Methods for Structural Optimization*, 1st ed.; Academic Press: Massachusetts, USA, 2017; pp. 27-46.
40. Alam, MS.; Sultana, N.; Hossain, SMZ., Bayesian optimization algorithm based support vector regression analysis for estimation of shear capacity of FRP reinforced concrete members. *Appl. Soft Comput.* **2021**, 105, 107281. https://doi.org/10.1016/j.asoc.2021.107281
41. Yang, L.; Shami, A., On hyperparameter optimization of machine learning algorithms: Theory and practice. *Neurocomputing* **2020**, 415, 295-316. https://doi.org/10.1016/j.neucom.2020.07.061
42. Su, Z.; Wang, Y.; Tan, B.; Cheng, Q.; Duan, X.; Xu, D.; Tian, L.; Qi, T., Performance prediction of disc and doughnut extraction columns using bayes optimization algorithm-based machine learning models. *Chem. Eng. Process.* **2023**, 183, 109248. https://doi.org/10.1016/j.cep.2022.109248
43. Snoek, J.; Larochelle, H.; Adams, RP, Practical Bayesian Optimization of Machine Learning Algorithms. *arXiv* **2012**. https://doi.org/10.48550/arXiv.1206.2944
44. Denk, L.; Hatta, H.; Misawa, A.; Somiya, S. Shear fracture of C/C composites with variable stacking sequence. *Carbon* **2001**, 39, 1505-1513. https://doi.org/10.1016/S0008-6223(00)00278-5
45. LS-DYNA manual R13.0 Vol I. Available online: https://www.dynasupport.com/manuals/ls-dyna-manuals/ls-dyna_manual_volume_i_r13.pdf (accessed on 9th Jan. 2023)
46. Tsai, S.W.; Melo, J.D.D., A unit circle failure criterion for carbon fiber reinforced polymer composites. *Compos. Sci. Technol.* **2016**, 123, 71-78. https://doi.org/10.1016/j.compscitech.2015.12.011